—

SUPPLEMENTARY INFORMATION

—

The *Letter to Nature* estimates the probability for gravitational lensing among high redshift galaxies, with emphasis on current surveys using the *HUDF*, and future surveys to be carried out using *JWST*. The *Letter* also uses the observed distributions of separation between very high redshift galaxy candidates in the *HUDF* and foreground galaxies, to show that a significant fraction of these objects are likely to be gravitationally lensed. The following sections expand the brief descriptions of the modelling and interpretation that can be found in the *Letter to Nature*.

1. Schematic Picture of Magnification Bias and Foreground Galaxy Correlation

In Supplementary Figure 1, we present a schematic representation of a portion of the *HUDF*, which shows how magnification bias leads to a correlation between foreground galaxies and high redshift candidates. Panel **a** shows a representation of the Schechter function[22], which describes the luminosity function (LF) of high redshift galaxies. The limiting absolute magnitude $M_{\rm lim}$ and characteristic magnitude $M_\star$ are shown for reference. Gravitational lensing magnifies sources relative to their intrinsic luminosity, and draws intrinsically faint galaxies into the flux limited sample. Since faint galaxies are much more common than bright galaxies, the number of sources per unit area in regions of lensing magnification is significantly higher. This leads to a bias of sources near foreground galaxies. To illustrate this effect on the high redshift galaxy samples in the *HUDF*, we sketch in panel **b** a portion of the sky approximately 10 arcseconds across. In this panel, background sources (i.e. high redshift galaxies) are shown in red and foreground galaxies (those near $z \simeq 1-2$) in blue. The faint galaxies (with $M_{AB} > M_{\rm lim}$) are signified by open symbols, while the closed symbols signify bright galaxies with $M_{AB} < M_{\rm lim}$. The black dotted disks denote regions of sky where background sources will be multiply-imaged by a foreground galaxy. For illustration, this schematic representation overestimates the total lensing cross-section, which is $\simeq 0.5\%$, by a factor of $\simeq 10$. The typical angular scale of these regions is 1 arc-second. We show those faint galaxies that lie within these lensing regions in green. In panel **c,** the faint galaxies that are close enough to bright foreground galaxies to be multiply-imaged (shown in green), producing in general a bright image with $M_{AB} < M_{\rm lim}$, and an undetected faint image with $M_{AB} > M_{\rm lim}$. Finally, the observed association of high redshift galaxies with bright foreground galaxies — once gravitational lensing bias has been accounted for — is

shown in panel **d**. In this example 2 of the 5 observed high redshift galaxies ($M_{AB} < M_{\rm lim}$) have entered the sample owing to gravitational magnification, and have close alignment with foreground galaxies as a result. In this case we find 40% of high redshift galaxies within $\simeq 1$ arc-second of bright foreground galaxies, even though the observed density of bright foreground objects is 1 per 20 square arcseconds. We note that gravitational lensing can also lower the observed density of sources on the sky that have neighbouring foreground galaxies by magnifying the angular extent of the image plane relative to the source plane. This effect, which is usually referred to as *depletion*, is not dominant when the LF is steep, as is the case for high redshift galaxies.

2. Lens Model

We refer to the a-priori probability for a galaxy at redshift $z_{\rm gal}$ to be multiply-imaged by an intervening foreground galaxy as the multiple image optical depth[17]

$$\tau_{\rm m} = \int_0^{z_{\rm gal}} \frac{d\tau_{\rm m}}{dz} dz, \tag{1}$$

where

$$\frac{d\tau_{\rm m}}{dz} = \int d\sigma \Phi(\sigma, z)(1+z)^3 \frac{cdt}{dz} \pi D_{\rm d}^2 \theta_{\rm ER}^2(\sigma, z), \tag{2}$$

$\theta_{\rm ER}$ is the Einstein radius as a function of velocity dispersion σ and redshift z, $D_{\rm d}$ is the angular diameter distance to the lens, and t is time. To calculate $\tau_{\rm m}$, we use the expression for the angular Einstein radius for a Singular Isothermal Sphere (SIS)

$$\theta_{\rm ER}(\sigma, z) = 0.9'' \, \frac{D_{\rm ds}}{D_{\rm s}} \left(\frac{\sigma}{161 {\rm km/s}} \right)^2, \tag{3}$$

where $D_{\rm s}$ and $D_{\rm ds}$ are the angular diameter distances to the source, and between the lens and source, respectively.

To evaluate $\Phi(\sigma, z)$, we first assume[26] the *Sloan Digital Sky Survey* (SDSS) velocity dispersion function[27] $\Phi_{\rm SDSS}(\sigma)$

$$\Phi_{\rm SDSS}(\sigma) d\sigma = \Phi_\star \left(\frac{\sigma}{\sigma_\star} \right) \frac{\exp\left[-(\sigma/\sigma_\star)^\beta\right]}{\Gamma(\alpha/\beta)} \beta \frac{d\sigma}{\sigma}, \tag{4}$$

where $\Phi_\star = 2 \times 10^{-3}\mathrm{Mpc}^{-3}$, $\alpha = 2.32$, $\beta = 2.67$ and $\sigma_\star = 161\,\mathrm{km/s}$. We further assume that the lens population has a constant co-moving density $\Phi(\sigma, z) = \Phi_{\mathrm{SDSS}}(\sigma)$. Although the density of galaxies must decline at high redshift, this approximation is reasonable, since most lensing occurs at $z \lesssim 1.5$. The uncertainty in predictions of the lens fraction owing to the unknown evolution of the velocity dispersion function is approximately a factor of two[26,31]. We note that this prescription gives a lensing cross-section for $z \simeq 2$ quasars that is consistent with the SDSS analysis[26], which is an observational requirement. The lens model assumes that galaxy velocity dispersions reach down to as low as $\sigma = 10\mathrm{km/s}$. However, as the lensing neighbours are selected by velocity dispersion, the distribution of lensed separations is not sensitive to the assumed cutoff, because the lens cross-section is proportional to velocity dispersion to the fourth power (σ^4).

We have utilised a simple lens model. In particular we have not included non-spherical lens distributions, which produce four rather than two image lenses in some cases. Indeed, empirical estimates for the fraction of quasar lenses that have four images of about 40% have been obtained from the homogeneous CLASS sample (`http://www.aoc.nrao.edu/~smyers/class.html`), and of about 15% from the Sloan Digital Sky Survey[32]. While the predicted four image to two image ratio depends on the ellipticity of the lensing galaxies[32], the ellipticity is found not to significantly influence the overall cross-section for multiple imaging[28,33,34]. On the other hand, the magnification bias can be larger for an elliptical lens, which would increase the expected multiple imaging rate[28]. Moreover, the additional images in a four image lens would increase the fraction of observed candidates that are part of a multiply-imaged galaxy. Using spherical lenses for our estimates is therefore conservative with respect the expected influence of gravitational lensing on samples of high redshift galaxy candidates, both in terms of the number of lenses predicted and the association between high redshift candidates and bright foreground galaxies. We note here that the lens population for $z \sim 8 - 10$ candidates is at higher redshift than the lens galaxies responsible for the aforementioned samples. However the measured ellipticity distribution is nearly constant over a very wide range of flux and redshift[35]. Thus, we argue that since our simple model provides a good statistical description of the available data, neglecting elliptical lenses is reasonable, particularly given the range of other uncertainties.

2.1. magnification bias

Flux limited samples are subject to magnification bias, which increases the relative probability that detected galaxies are gravitationally lensed[17], and concentrates sources in a flux limited sample around foreground objects[18]. Yan et al.[4] have observed a number of

$z \simeq 8-10$ candidates that have neighbouring bright foreground galaxies. As discussed in the *Letter*, this correlation is likely to be the manifestation of these effects. The magnification bias for sources with observed luminosities between L and $L + dL$ is

$$B(L) = \frac{\int_{\mu_{\rm min}}^{\mu_{\rm max}} \frac{d\mu}{\mu} \frac{dP}{d\mu} \Psi(L/\mu)}{\Psi(L)}, \tag{5}$$

while the corresponding overall magnification bias in a flux limited sample is

$$B_{\rm lens} = \frac{\int_{\mu_{\rm min}}^{\mu_{\rm max}} d\mu \int_{L_{\rm lim}}^{\infty} dL \frac{dP}{d\mu} \Psi(L/\mu)}{\int_{L_{\rm lim}}^{\infty} dL \frac{dP}{d\mu} \Psi(L)}, \tag{6}$$

where $dP/d\mu$ is the probability distribution for magnification (μ) within the range $\mu_{\rm min} < \mu < \mu_{\rm max}$. Of relevance for high redshift surveys in the *HUDF* or with *JWST* (which have an angular resolution much better than the image separation[30]) is the magnification distribution for the brighter image

$$\frac{dP_{\rm m,1}}{d\mu} = \frac{2}{(\mu-1)^3} \quad \text{for} \quad 2 < \mu < \infty. \tag{7}$$

We adopt a Schechter[22] function for the LF

$$\Psi(L)dL = \Psi_\star \left(\frac{L}{L_\star}\right)^\alpha \exp\left(-\frac{L}{L_\star}\right)\frac{dL}{L_\star}, \tag{8}$$

where $\Psi_\star$ is the characteristic density in Mpc^{-3}, and α is the power-law slope at luminosities below the characteristic break at $L_\star$. Below, and in the *Letter*, we quote the characteristic luminosity in terms of the absolute magnitude $M_\star = M + 2.5 \log_{10} L/L_\star$.

2.2. gravitationally lensed luminosity function

We note that in the presence of significant gravitational lensing, the LF can be modified from its intrinsic form[23], leading to a power-law slope at the bright-end of -3 (as shown in Figure 3 of the *Letter*). The modified LF can be estimated by modelling the overall magnification distribution using the probability distribution for magnification of multiply-imaged sources over a fraction $\tau_{\rm m}$ of the sky, combined with a de-magnification $\mu_{\rm demag} =$

$(1 - \langle\mu_{\rm mult}\rangle\tau_{\rm m})/(1 - \tau_{\rm m})$ elsewhere. Here $\langle\mu_{\rm mult}\rangle = 4$ is the mean magnification of multiply-imaged sources, and $\mu_{\rm demag}$ has been calculated in order to conserve flux on the cosmic sphere centred on an observer. The modified LF can then be approximated using the expression

$$\Psi_{\rm obs}(L) = (1-\tau_{\rm m})\frac{1}{\mu_{\rm demag}}\Psi(L/\mu_{\rm demag}) + \tau_{\rm m}\int_0^\infty d\mu \frac{1}{\mu}\left(\frac{dP_{\rm m,1}}{d\mu} + \frac{dP_{\rm m,2}}{d\mu}\right)\Psi(L/\mu), \quad (9)$$

where $dP_{\rm m,2}/d\mu = 2/(\mu+1)^3$ for $0 < \mu < \infty$, is the probability distribution for the second image. We approximate the true magnification distribution by using a constant value of $\mu_{\rm demag}$ in regions of no multiple imaging. This is valid for the modification of the LF at luminosities much brighter than $M_\star$, in which we are interested in this work.

3. Lensing Predictions for High Redshift Surveys

We summarise the predictions of our lensing model in Supplementary Figure 2. As shown in panel **a**, the lensing optical depth rises toward high redshift[11], and is 4-5 times as large for sources at $z \simeq 6$ as at $z \simeq 1.5$. It doubles again from $z = 6$ to $z = 20$, so that at $z > 10$ the multiple imaging fraction is greater than 0.5%, even in the absence of magnification bias. Panel **b** shows the magnification bias as a function of the difference between $M_\star$ and the survey limit in absolute magnitude $M_{\rm lim}$. At low redshifts, deep surveys can probe well below $M_\star$, so that the magnification bias is dominated by the power-law slope (α) of the Schechter function at low luminosities, and the resulting bias is of order unity. At very high redshifts, however, current surveys can only reach $M_\star$ or even brighter, and hence the bias can be much higher (tens or hundreds) owing to the exponential nature of the LF sampled. We next combine the optical depth $\tau_{\rm m}$ with the bias $B_{\rm lens,1}$ to find the multiple image fraction $F_{\rm lens} = B_{\rm lens,1}\tau_{\rm m}/(B_{\rm lens,1}\tau_{\rm m} + (1-\tau_{\rm m}))$, where we have assumed the bias of those galaxies which are not multiply-imaged to be unity. In panel **c** we plot contours of $F_{\rm lens}$ as a function of z and $(M_\star - M_{\rm lim})$. Surveys at low redshift ($z \lesssim 3$), with limits fainter than $M_\star$, should have multiple image fractions below 1%. However, at higher redshifts the lens fraction can be much higher. For example, a survey at $z \gtrsim 6$ that reaches only 1 magnitude brighter than $M_\star$ could have a lens fraction of 10%. Current and future surveys at $z > 6$ with *HST* and *JWST* lie in this upper-right portion of panel **c**. Only ultradeep surveys with *JWST* that reach well below $M_\star$ at $z \gtrsim 10$ will have their lensing fraction drop well below 10% again.

4. High Redshift Galaxy Candidate Samples

To compare the predictions of our model with samples of high redshift galaxy candidates, we investigate samples from the *HUDF* compiled by Yan et al.[4]. These and other authors have employed the Lyman-break (or *dropout*) technique to select galaxies at $z \gtrsim 7$ in the *HUDF*. We note that the major colour criteria used to select the samples of Yan et al.[4] are very similar to those employed by other groups including Bouwens et al.[1,3]. However the overlap of individual candidates among the samples from these two teams is small. In particular, none of J-dropouts compiled by Yan et al.[4] are among the three J-dropouts presented by Bouwens et al.[1]. There could be a range of reasons for this disjoint. With respect to our current work, we note that one reason for the difference in sample selection could be the choice of whether to include candidates near bright foreground objects. By construction, the samples of Yan et al.[4] were not biased against regions around foreground objects, indicating that *if* gravitationally lensed, multiply-imaged galaxies do exist in the *HUDF* at $z \sim 8-10$, then they would be selected. We therefore concentrate here on the predicted gravitational lensing statistics for these samples.

The $z \approx 8.6$ sample used to discuss the gravitational lensing of galaxies in the *HUDF* as part of this work consists of 15 Y-dropouts (spanning the redshift range of $7.7 \lesssim z \lesssim 9.4$), while the $z \approx 10.6$ sample consists of 20 J-dropouts (spanning $9.4 \lesssim z \lesssim 11.8$). These objects are all very faint, and have magnitudes ranging from $M_{\rm AB} = 28.0 - 29.0$.

4.1. lensing predictions for $z \simeq 8-10$ candidates

We have calculated multiple-imaging probabilities for the $z \simeq 8-10$ samples[4] as a function of galaxy absolute magnitude assuming $M_\star = -17.8$ mag. These results can be used to discuss lensing probabilities for individual $z \simeq 8-10$ dropout candidates[4] in more detail.

Panel **a** of Supplementary Figure 3 shows the probability that a galaxy with absolute magnitude $M_{AB,1}$ is multiply-imaged. At $z \simeq 6-7$, only galaxies much brighter than $M_{AB,1} < -21$ mag have a significant chance of being lensed. However, at $z \simeq 8-10$ galaxies as faint as $M_{AB,1} \simeq -19$ mag have a substantial lens fraction. Of course, these are just statements reflecting the relative brightness of $M_{\rm lim}$ and M_*. Our results suggest that a number of $z \simeq 8-10$ galaxies detected in the *HUDF* should be multiply-imaged. On the other hand, we note that we have not identified any image pairs in the *HUDF*. Panel **b** shows the probability that a *lensed* galaxy with observed $M_{AB,1}$ has a corresponding *second* image with $M_{AB,2} < M_{\rm lim}$, such that it is also detectable above the *HUDF* flux limit. For this

probability to be large ($\gtrsim 50\%$), the detected image must be more than $\simeq 1$ mag brighter than $M_{\rm lim}$. Panel **c** shows the fraction of galaxies that are part of a lensed pair in which *both* images are detectable, $[F_{\rm dbl} = F_{\rm lens} \times P(M_{AB,2} < M_{\rm lim}|M_{AB,1})]$. We find that at $z \simeq 6-7$, only galaxies that are several magnitudes brighter than $M_{\rm lim}$ have a reasonable chance (few-10%) of being observed as a multiple image system. However, at $z \simeq 8-10$, this probability increases to $\gtrsim 10\%$ for galaxies that are only a magnitude brighter than $M_{\rm lim}$.

We note that the predicted fraction would increase if we modelled elliptical lenses which can have more than two images. We roughly estimate the fraction in this case by noting that a four-image lens typically has either two bright images of approximately equal magnification where the source is near a fold caustic, or three bright images with the central one having a magnification equal to the sum of the other two[36] . Thus, close to the detection limit, we expect either the two bright images, or only the brightest of three bright images would be detected for typical four-image lenses. We therefore argue that for the (empirically observed) 15-40% of cases where the lens has four images, the fraction of multiply-imaged systems in which more than one image is detected will increase by at most a factor of approximately two.

In Supplementary Figure 3, we have superimposed squares to show probabilities for individual galaxy candidates in the *HUDF* [4] . We use $M_\star = -17.8$ mag estimated by Yan et al.[4] as an example. By summing probabilities for individual galaxy candidates in the Yan et al.[4] sample, we calculate the (mean) expected number of lensed systems, finding $\langle N_{\rm lens}\rangle = 0.8 \pm 0.1$ and $\langle N_{\rm lens}\rangle = 1.7 \pm 0.2$ among the 15 and 20 candidates at $z \simeq 8.6$ and $z \simeq 10.6$, respectively. If the true $M_\star$ value is fainter, these numbers will be higher. A Poisson distribution with mean $\langle N_{\rm lens}\rangle = 2.5$ implies that at least one lens pair would be found among the observed $z \simeq 8-10$ sample in 92% of cases, which stands in apparent contrast to the fact that no image pairs have been identified in the *HUDF*. However, we find the probability that a *lensed* galaxy with observed $m_{AB,1}$ has a corresponding *second* image with $m_{AB,2} < m_{\rm lim}$ (i.e. detectable with the *HUDF* data) to be only $\simeq 10\%$, even for galaxies that are one magnitude brighter than $M_{\rm lim}$. Here we neglect the caveat that secondary images could fall on top of the foreground galaxies, which would further reduce the chance of their being observed. We estimate that the number of systems that would be observed as doubles (i.e. both images detected) to be $\langle N_{\rm dbl}\rangle = 0.2 \pm 0.06$ and $\langle N_{\rm dbl}\rangle = 0.4 \pm 0.1$ at $z = 8.6$ and 10.6, respectively. A Poisson distribution with mean $\langle N_{\rm dbl}\rangle = 0.6$ implies that the observed $z \simeq 8-10$ sample would not contain any doubles in most (55%) cases. Thus, with $M_\star = -17.8$, we find that $N_{\rm lens} \simeq 2-3$ of the detected galaxies in each redshift range should be multiply-imaged, but do not necessarily expect any of these to be identified as multiple image systems. On the other hand, an even fainter value of $M_\star = -17.3$ (-17.1) implies that at least one double would be observed in 90% (99%) of cases, imposing an upper-limit

of $M_\star \lesssim -17$ at $z \sim 8-10$. We note that the values of $M_\star$ — as measured — could also be biased by gravitational lensing (see Figure 3 of the *Letter*). Currently, none of the published LFs at $z \gtrsim 7$ are corrected for the potential lensing bias. However it is clear from the results presented in our *Letter*, that such corrections will need to be prescribed in detail in the future.

The mean magnification of detected lensed images (with $M_\star = -17.8$) is $\langle\mu\rangle \simeq 6$, indicating that gravitational lensing in these samples would lead to over-estimates of the luminosity density at $z \simeq 8.6$ and $z \simeq 10.6$ of $\simeq 50\%$ and $\simeq 80\%$, respectively, if the magnification is neglected. Since the axis ratio of lensed images is equal to the magnification for an SIS, this also implies that the lensed images should be significantly elongated, and indeed some candidates appear to have this property[4] . However, the signal-to-noise for the detected candidates is too low to draw quantitative conclusions.

5. Distribution of Lensed Separations

As shown in the previous section, we find that in most cases only the more magnified image will be brighter than the detection threshold. We therefore calculate the expected distribution of angular separation between a lens galaxy and the brighter of the two images. The apparent angular separation of the bright image with magnification μ from the center of a lensing SIS at redshift $z < z_{\rm gal}$ is

$$\Delta\theta_{\rm lens}(\mu, z) = \left(1 + \frac{1}{\mu - 1}\right)\theta_{\rm ER}(z). \tag{10}$$

Using this expression we evaluate the probability distribution for the separation of bright images of image pairs from the lensing galaxy

$$\frac{dP}{d\Delta\theta} \propto \int_0^{z_{\rm gal}} dz \int_2^\infty d\mu \int_{L_{\rm lim}}^\infty dL \frac{d\tau_{\rm m}}{dz}\frac{dP_{\rm m,1}}{d\mu}\Psi(L/\mu)\delta_{\rm dir}([\Delta\theta - \Delta\theta_{\rm lens}(\mu, z)], \tag{11}$$

where $\delta_{\rm dir}$ is the Dirac delta function, and $L_{\rm lim}$ is the unlensed luminosity corresponding to the survey flux limit.

6. Observed Correlation Between High Redshift Candidates and Foreground Galaxies

For comparison with the lensing predictions, we measure the distribution of separations between $z \simeq 8-10$ candidates[4] and their nearest bright ($H \leq 25$ mag) foreground galaxy. The red histograms in panels **a** of Supplementary Figures 4 and 5 show the cumulative distributions of this separation for the $z \simeq 8.6$ and $z \simeq 10.6$ candidates, respectively. Comparing the distributions in these two panels with the random line-of-sight and lensed predictions, two trends are obvious. Firstly, these $z \simeq 8-10$ candidates are observed to be closer to bright foreground galaxies than are random lines-of-sight. On the other hand, the candidates are found at larger separations from foreground galaxies than would be predicted if they were all multiply-imaged. Quantitatively, the Kolmogorov-Smirnov probabilities ($P_{\rm KS}$) between the observed distributions and the *all-random* model or the *all-lensed* model (labeled in the figure) indicate that either model is rejected at high significance. This suggests that a fraction of these candidates may be gravitationally lensed.

For illustration, the thick black lines in panels **a** of Supplementary Figures 4 and 5 show the composite distributions corresponding to multiple image lens fractions of $F_{\rm lens} = 0.2$ and 0.4, at $z \simeq 8.6$ and 10.6, respectively. These provide an excellent fit to the data ($P_{\rm KS}$ values labeled in Supplementary Figures 4 and 5). Panels **b** of Supplementary Figures 4 and 5 show the differential distributions of the observed angular separations (red), as well as the corresponding composite models (thick black) and the random distributions (dotted black). The latter demonstrates that the largest observed separations can be attributed to a random distribution.

We next examine the redshift distributions of the nearest bright foreground galaxies, using spectrophotometric redshift estimates[37] . The cumulative distributions are compared in panels **c** of Supplementary Figures 4 and 5 for the $z \simeq 8.6$ and 10.6 candidates, respectively. The red histograms are the distributions for the neighbours of the high redshift candidates, the dotted black lines are distributions for the neighbours of random lines-of-sight, and the dashed black lines are distributions for the expected gravitational lens redshift[17]. The redshift distributions of the foreground galaxies associated with the full samples of $z \simeq 8-10$ candidates cannot be differentiated from those associated with random lines-of-sight. In addition, for the $z \simeq 10.6$ case in particular, foreground galaxy redshifts are found not to be drawn from a lensed galaxy population. However, the lens angular separation cuts off sharply at $\Delta\theta \simeq 1.5$ arcseconds. We therefore generate the distribution of redshifts only for foreground galaxies found within $\Delta\theta < 1.5$ arcseconds of the $z \simeq 8-10$ candidates, which are shown as the blue histograms in these two panels. These distributions are consistent with the distribution of gravitational lens redshifts, which supports the hypothesis that many

close candidate–foreground galaxy pairs in this sample result from magnification bias. In panels **c** and **d** of Supplementary Figures 4 and 5, we show the model redshift distributions corresponding to the values $F_{\rm lens} = 0.2$ and 0.4 for candidates at $z \simeq 8.6$ and 10.6, respectively (thick black lines). These again provide an excellent fit to the data, which, when taken together with the correlation between high redshift and foreground galaxy positions, provides compelling evidence for a significant lens fraction among the $z \gtrsim 8$ galaxy candidates, since these foreground galaxies were selected only on the basis of their alignment with high redshift candidates.

REFERENCES

[31] Chae, K. Galaxy evolution from strong-lensing statistics: the differential evolution of the velocity dispersion function in concord with the Λ cold dark matter paradigm. *Mon. Not. R. Astron. Soc.* **402**, 2031–2048, (2010).

[32] Oguri, M. Is there a quad problem among optical gravitational lenses? *New J. of Phys.* **9**, 442–450, (2007).

[33] Blandford, R. D. and Kochanek, C. S. Gravitational imaging by isolated elliptical potential wells. I - Cross sections. II - Probability distributions. *Astrophys. J.* **321**, 658–675, (1987).

[34] Kochanek, C. S. The flat-spectrum radio luminosity function, gravitational lensing, galaxy ellipticities, and cosmology. *Astrophys. J.* **473**, 595–609, (1996)

[35] Odewahn, S., Burstein, D., and Windhorst, R. A. The axis ratio distribution of local and distant galaxies. *Astron. J.***114**, 2219–2231, (1997)

[36] Mao, S. Gravitational microlensing by a single star plus external shear. *Astrophys. J.* **389**, 63–67, (1992).

[37] Ryan, Jr., R. E., Hathi, N. P., Cohen, S. H., Malhotra, S., Rhoads, J., Windhorst, R. A., Budavári, T., Pirzkal, N., Xu, C., Panagia, N., Moustakas, L. A., di Serego Alighieri, S., and Yan, H. The Galaxy Luminosity Function at $z \sim 1$ in the *HUDF*: Probing the Dwarf Population. *Astrophys. J.* **668**, 839–845, (2007).

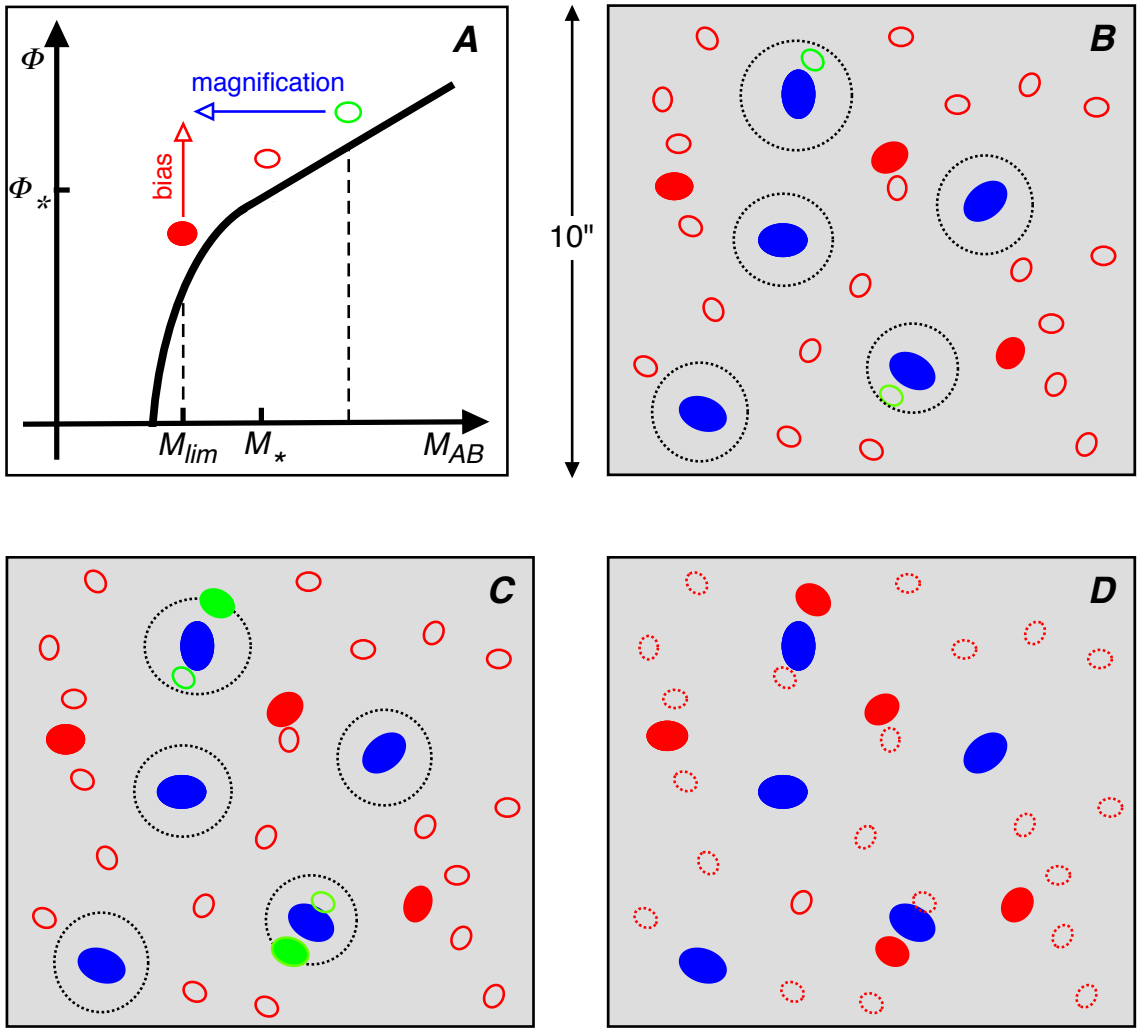

Supplementary Figure 1. **Schematic representation showing how magnification bias leads to an association between foreground galaxies and high redshift candidates. Panel a:** The Schechter LF of high redshift galaxies. **Panel b:** High redshift galaxies (red) and foreground galaxies (blue). Faint galaxies (those with $M_{AB} > M_{\rm lim}$) are signified by open symbols, while the closed symbols signify bright galaxies with $M_{AB} < M_{\rm lim}$. The black dotted disks denote regions of sky where background sources will be multiply imaged by the foreground galaxy. Faint background galaxies that lie within these lensing regions are shown in green. **Panel c:** The lensed faint galaxies are multiply-imaged, producing a bright image with $M_{AB} < M_{\rm lim}$, and an undetected faint image with $M_{AB} > M_{\rm lim}$. Galaxies located near the lines of sight to foreground galaxies that are not multiply imaged, are deflected to larger separations, resulting in a lowering of observed source density (an effect known as depletion). **Panel d:** The correlation of observed high redshift galaxies (solid red symbols) with bright foreground galaxies once gravitational lensing bias has been accounted for. The depletion effect is opposite in sign to the correlation introduced through strong lensing, but is sub-dominant in the case of high redshift galaxies.

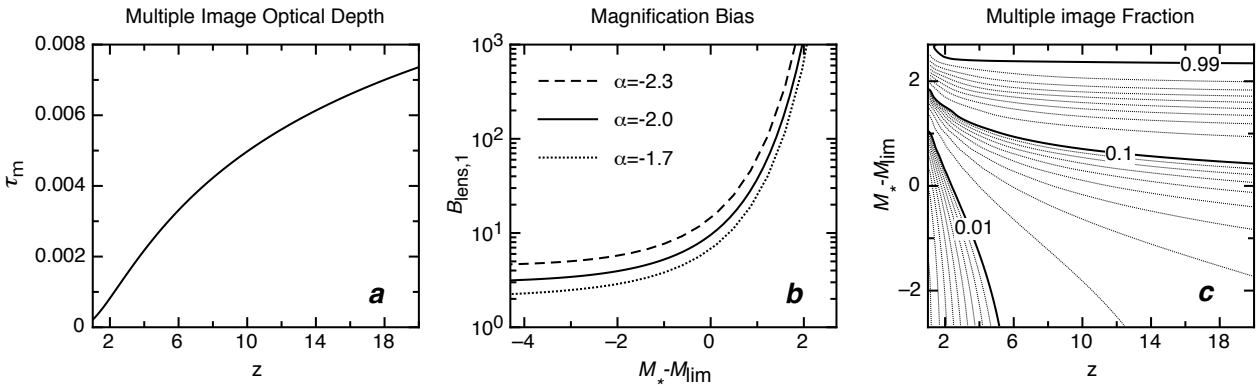

Supplementary Figure 2. **Probabilities for multiple imaging of high redshift galaxies. Panel a:** The lensing optical depth as a function of redshift. **Panel b:** The magnification bias as a function of the difference between $M_\star$ and the limiting survey absolute magnitude $M_{\rm lim}$. Three values of the faint-end LF-slope α are considered. **Panel c:** Contours of $F_{\rm lens}$ as a function of z and $(M_\star - M_{\rm lim})$, assuming[1] $\alpha = -2$.

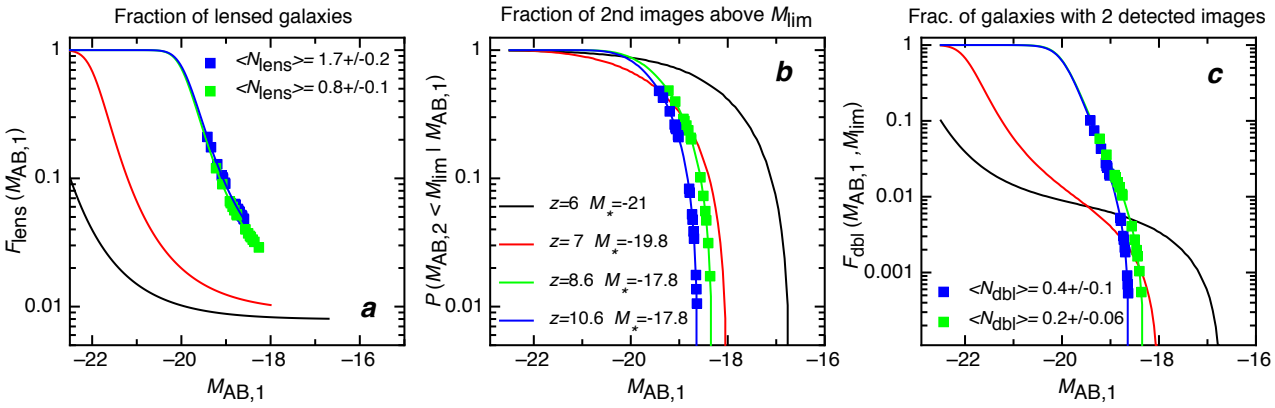

Supplementary Figure 3. **Probabilities for multiple imaging of $z \simeq 8-10$ galaxy candidates. Panel a:** The probability that a galaxy with observed $M_{AB,1}$ is multiply-imaged. The expected mean number of lenses ($\langle N_{\rm lens}\rangle$) among the $z \simeq 8.6$ and $z \simeq 10.6$ candidates is listed. **Panel b:** The probability that a *lensed* galaxy with observed $M_{AB,1}$ has a corresponding second image with $M_{AB,2} < M_{\rm lim}$. **Panel c:** The fraction of galaxies that are part of a lensed pair in which both images are detectable (68% errors here were computed using a bootstrap method). The expected mean number of systems that would be observed as doubles ($\langle N_{\rm dbl}\rangle$) is listed. We have assumed the determinations of $M_\star = -17.8$ and $\alpha = -2$, and observed absolute magnitudes $M_{AB,1}$ from Yan et al.[4] (the squares correspond to probabilities for the individual galaxy candidates).

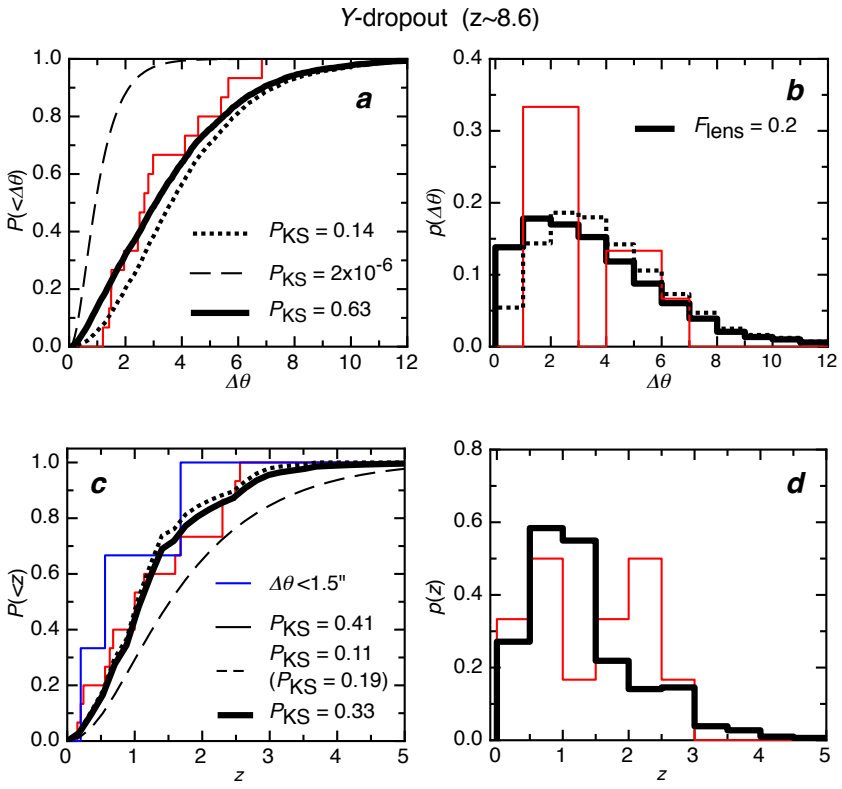

Supplementary Figure 4. **Probability distributions for angular proximity and redshift of bright foreground galaxies among the sample of $z \sim 8.6$ candidates. Panel a:** The cumulative distribution for the angular separation between $z \simeq 8.6$ candidates and their nearest foreground galaxies with $H \leq 25$ in the *HUDF* (red histogram). Also shown are the model cumulative distributions of angular separations between *random* lines-of-sight and the nearest bright foreground galaxies (dotted black line), and of angular separations for the brighter image of gravitationally *lensed* objects at $z = 8.6$ (dashed black line). The thick black line shows the composite cumulative distribution generated by summing the *random* and *lensed* histograms, with a weight equal to a lens fraction of $F_{\rm lens} = 0.2$. **Panel b:** The binned histograms (area normalised to unity) for the angular separations of observed candidates (red), for separations in the composite model (thick black), and for separations from random lines of sight (dotted black). **Panel c:** The cumulative redshift distribution for foreground galaxies associated with $z \simeq 8.6$ candidates (red histogram). Also shown are the cumulative distributions for the redshifts of foreground galaxies nearest to *random* lines of sight (dotted black line), and for the expected gravitational lens redshifts assuming sources at $z = 8.6$ (dashed black line). The thick black line shows the composite cumulative distribution ($F_{\rm lens} = 0.2$). We also plot the redshift distribution of foreground galaxies within 1.5 arcseconds of a $z \simeq 8.6$ candidate (blue histogram). **Panel d:** The binned histograms for the foreground galaxy redshifts along lines of sight to dropout candidates (red), and for the composite model (black). In each case, values of $P_{\rm KS}$ corresponding to the comparison of the data with the model distributions are listed.

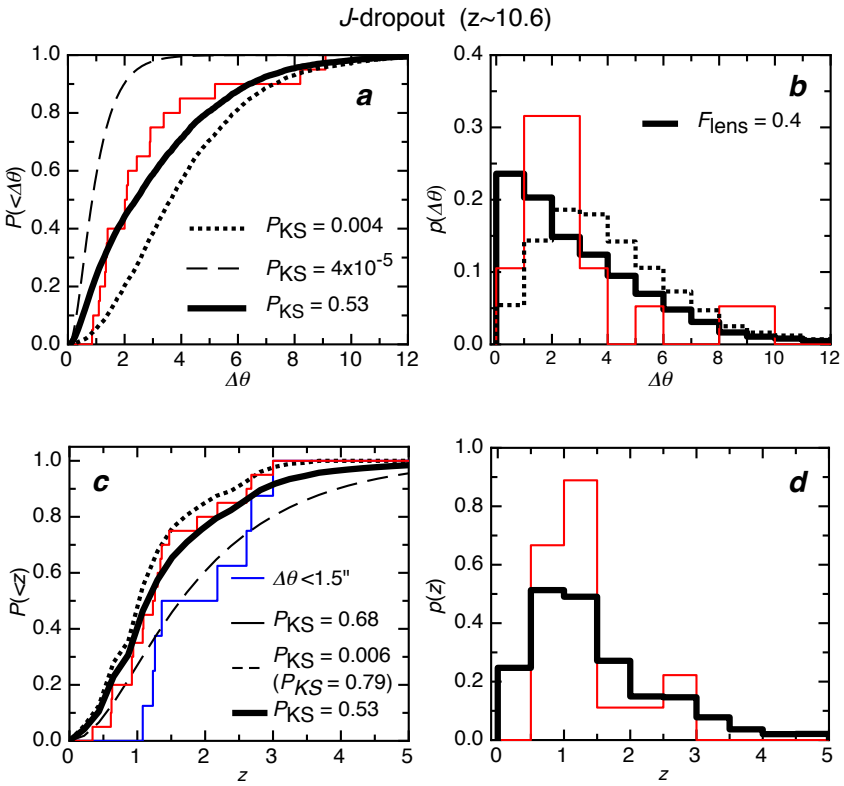

Supplementary Figure 5. **Probability distributions for angular proximity and redshift of bright foreground galaxies among the sample of $z \sim 10.6$ candidates.** The panels mirror those of Supplementary Figure 4. We assume $F_{\rm lens} = 0.4$ for the model composite distribution.